Research Article

Detection of microplastics and nanoplastics released from a kitchen blender using Raman imaging

Yunlong Luo [a], Olalekan Simon Awoyemi [a], Ravi Naidu [a,b], Cheng Fang [a,b,*,1]

[a] *Global Centre for Environmental Remediation (GCER), University of Newcastle, Callaghan, NSW 2308, Australia*
[b] *Cooperative Research Centre for Contamination Assessment and Remediation of the Environment (CRC CARE), University of Newcastle, Callaghan, NSW 2308, Australia*

HIGHLIGHTS

- Raman imaging identifies acrylonitrile butadiene styrene micro- and nanoplastics.
- The PCA/algebra-based algorithm min- imises bias for plastic identification.
- Image re-construction via Gaussian fitting helps to reduce the noise in Raman maps.
- Billions of plastic fragments may be released during 30-second blending.

GRAPHICAL ABSTRACT
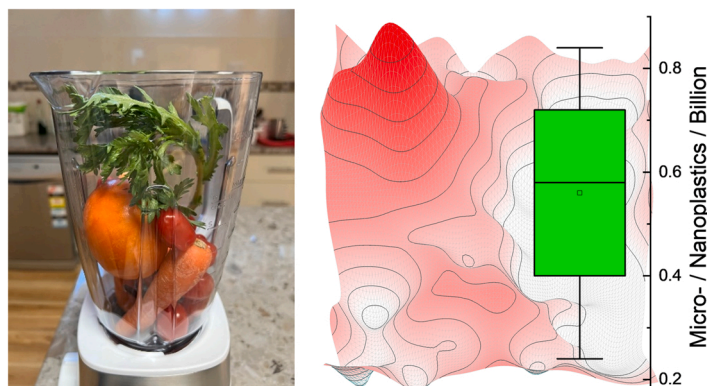
ABSTRACT

Microplastics and nanoplastics have secretly entered our daily lives but the extent of the problem is still unclear, as the characterisation is still a challenge, particularly for nanoplastics. Herein we test a blender that we use in our kitchen to make juice and we find that a significant amount of microplastics and nanoplastics ($\sim$0.36–0.78 $\times$ 10^9 within 30 s) are released from the plastic container. We advance the characterisation of microplastics and nanoplastics using Raman imaging to generate a scanning spectrum matrix, akin to a hyperspectral matrix, which contains 900 spectra (30 $\times$ 30). By mapping these hundreds of spectra as images, with help of algorithms, we can directly visualise the microplastics and nanoplastics with an increased sensitivity from statistical point of view. Raman imaging has a main disadvantage of the imaging resolution, originating from the diffraction of the laser spot, which is proposed to be improved by shrinking the scanning pixel size, zooming in the scanning area to capture details of nanoplastics. Using image re-construction towards deconvolution, the nanoplastics can be effective characterised and the bumpy image of microplastics stemming from the signal variation can be sub-sequently smoothened to further increase the signal-noise ratio. Overall, the advancements on Raman imaging

* Corresponding author at: Global Centre for Environmental Remediation (GCER), University of Newcastle, Callaghan, NSW 2308, Australia.
  E-mail address: cheng.fang@newcastle.edu.au (C. Fang).
[1] https://orcid.org/0000-0002-3526-6613

can provide a suitable approach to characterise microplastics and nanoplastics released in our daily lives, for which we should be cautious.

1. Introduction

The proliferation of plastic products over the past several decades raises problems in numerous areas of our society. Accumulation of synthetic plastic waste in the environment threatens living organisms and their habitats, potentially posing a significant risk to biodiversity [7]. This worrying trend will continue in the foreseeable future, due to people's heavy reliance on the plastic and the low recycling rate [14]. Once in the environment, plastic products may break down over time and release small fragments as microplastics (<5 mm) and nanoplastics (<1 μm) [8]. Compared with large pieces of plastic waste, these tiny plastic contaminants can be more detrimental to the natural environment. Since these contaminants have the large specific surface area due to their small sizes and large quantities, microplastics and nanoplastics are able to carry a variety of harmful chemicals [12]. Eventually these contaminants can move through the food chain and return to humans [11].

In addition to being environmental contaminants, microplastics and nanoplastics are also released and present in our daily lives. An increasing number of indoor microplastic sources have been identified in recent years, such as clothing made from synthetic materials [26], personal care products, food packaging, kitchenware and gardening tools [1,19]. These contaminants can be created as a consequence of the fragmentation of plastic items through strong mechanical force (e.g., cutting, shredding, scuffing, and abrasion), weathering, ageing and degradation [15,22]. Given that people spend up to 90% of their time indoors, health risks due to exposure to microplastics and nanoplastics indoors in our daily lives should not be overlooked [21]. Unfortunately, the current understanding is still very limited.

The kitchen is one place where plastic can be easily found. Plastic products are generally durable and lightweight, and using them has become a way of our daily lives [10]. Plastic kitchenware and appliances are useful for performing common household activities, such as preparation, processing, serving and storage of food and beverages. As a group of popular kitchen appliances, blenders are versatile tools to mix food and liquid, and some of them have the function of crushing hard objects, such as coffee beans, ice and frozen ingredients. A blender has a motor that drives a sharp stainless steel blade to chop objects in a jar or container [16]. The intense spiral motion produces a significant shear force likely resulting in friction between the chopped objects and the inner wall of the plastics container [17]. Such an interaction can affect the integrity of the plastic material and release unwanted plastic debris into the food or juice, leading to microplastics and even nanoplastics contamination concerns. However, to investigate this possibility and the extent of microplastic or nanoplastics released, an effective analytical method needs to be employed.

Several technologies are available for identifying micro-/nanoplastics, with common ones including microscopy, pyrolysis gas chromatography/mass spectrometry, Fourier transform infrared spectroscopy (FTIR), and Raman spectroscopy [8]. Microscopic inspection is usually performed in the first step to enable identification of the suspected particles, but a further step is needed to confirm the chemical character of the particles. Raman spectroscopy is one of the most powerful analytical methods, especially when it comes to characterising the small fraction of microplastics (<20 μm) and nanoplastics [2,9]. The high resolution of Raman microscopy enables the visualisation of particles even in the nanometre range (down to 100 nm) by mapping the scanning spectrum matrix that are collected pixel-by-pixel towards imaging [20]. Raman imaging can also identify plastic additives and pigments that might have harmful biological effects as well [27]. Although Raman imaging is deemed an effective analytical method for microplastics and nanoplastics, more work remains to be done to validate and optimise this technology.

This study aims to advance the characterisation of microplastics and nanoplastics by researching plastic fragments created under high shear force applied in a blender. We adjust Raman imaging parameters to visualise this distinctive form of microplastics and nanoplastics. Several algorithms, such as algebra-based and principal component analysis (PCA), are used to process the scanning spectrum matrices (akin to a hyperspectral matrix), to enhance signal recognition towards imaging. After imaging, in order to address several important technical problems, such as imaging resolution limit and signal variation resulting from an uneven sample surface, we develop another algorithm towards image reconstruction that is similar to FIONA—fluorescence imaging with one-nanometre accuracy [24]. Overall, the findings obtained from this work will contribute to the progress of Raman imaging application in the realm of microplastics and nanoplastics. The results also extend the existing scientific knowledge of indoor plastic contamination, highlighting an urgent need for comprehensive risk assessment.

## 2. Materials and methods

2.1. Chemicals and samples

All chemicals including ethanol and acetone were purchased from Sigma-Aldrich (Australia) and used as received. Milli Q water (>18 MΩ•cm) was used for the analysis. The blender was purchased from a local supermarket (BigW, Australia), and shown in Fig. S1 (Supporting Information).

All virgin microplastics (beads or pellets, usually with diameters < 1 mm) including polystyrene (PS), polyethylene terephthalate (PET), polyethylene (PE), polyvinyl chloride (PVC) and polypropylene (PP) were purchased from Sigma-Aldrich (Australia) and used as received. Several Raman spectra were extracted from the database when the standard plastic targets were not available, inducing polyamide (PA or PA 6), poly(methyl methacrylate) (PMMA), polycarbonate (PC, be careful, it is different from the principal components of PCA, marked as PC# in this study, such as PC1, PC2 etc.), polyurethane (PUR), and acrylonitrile butadiene styrene (ABS).

Before test, the blender was cleaned in turn with tap water, boiling water, ethanol and MQ water. The wall of the container was scratch using a stainless knife to collect some debris as "mother" material, which acted as reference for our test.

To mimic the blending process and simplify the sample preparation, we used MQ water to generate ice block in a refrigerator. We then mixed 12 pieces of ice blocks (~10 mL each) of with MQ water to ~500 mL, and blended them immediately, without food or fruit, using the pause function (1 s period of working and 1 s period of halting). During the blending process, we noted that the ice usually disappear/melt within 30 s. After that, we transferred the ~500 mL liquid to a glass beaker (2–5 L) (previously cleaned with MQ water, acetone, ethanol with help of sonication), boiled them to nearly dry. We then washed the beaker with MQ water for 3 times and collected the liquid of ~15 mL. From this concentrated liquid (from 500 mL to 15 mL), we took a droplet of ~5 μL and deposited onto a glass slide surface that had been previously cleaned by dipping into piranha solution (1:1 H_2SO_4: H_2O_2, v/v. *Be cautious, this solution reacts vigorously with organics*). After drying in room temperature, the Raman test was followed. Each test was conducted in duplicate.

Although the mimicked process is different from real situations, this study can lead to a better understanding on the likelihood of the releasing microplastics and nanoplastics from the cooking ware in our kitchen. For QC/QA control, we blend the MQ water for 0 s and 30 s, and
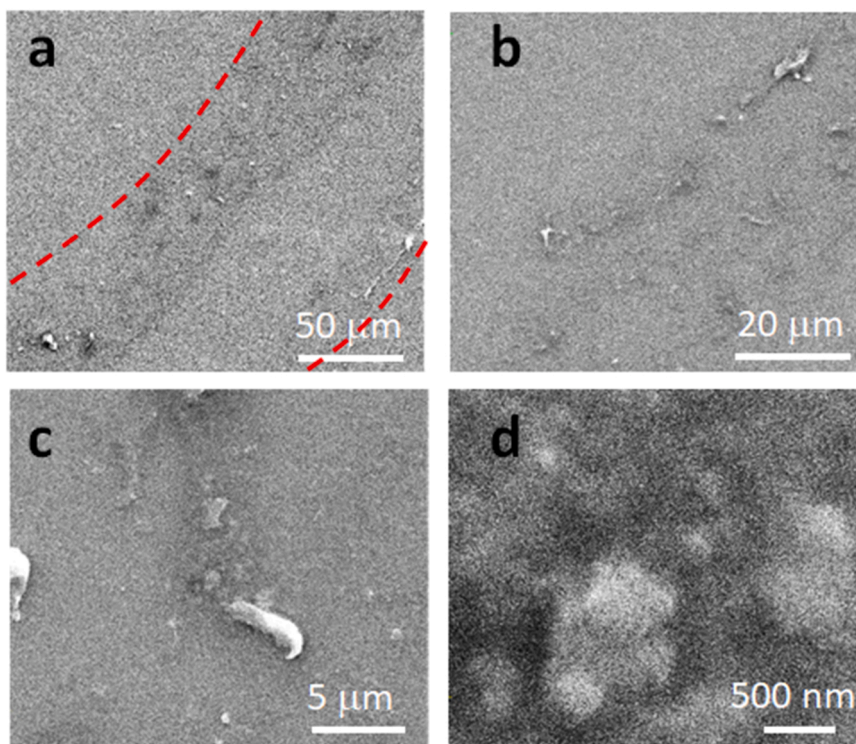
Fig. 1. SEM images under different magnifications, recorded on glass surface from the boundary of the "coffee ring", left behind by a droplet of ~5 µL. (a) shows the overview of the coffee ring. (b-d) show the details. (The "coffee ring" effect is the phenomenon as follows: when a liquid droplet dries up on a surface, the suspended particles in the liquid have the tendency to drift outwards from the centre and concentrate at the outer rim of the droplet).

kept the ice/MQ water static for 30 s as well. The same protocol was followed to test the particles as controls. In general, we did not get the significant amount of particle as we reported below. To minimise the alien particles, cotton clothing or lab coat were worn and plastic containers and tools were avoided wherever possible. Glass sample containers were used and covered with aluminium foil. Prior to working commencing, work surfaces were cleaned using Milli Q water and ethanol. Experiments were conducted in the fume hood where possible.

Different brands of blenders might generate the varied results, due to different materials, working mortar/speed/function, conditions (dry or wet) and configurations. We understand that the manufacturers intend to select the hard plastic materials with anti-fraction properties, to minimise the releasing particles during the blending process. The blender we tested herein has the container of plastics, which obviously is not made of glass or stainless steel.

2.2. Testing protocols and data analysis algorithms

The testing protocols were following the previous study [20]. In brief, Raman spectra were recorded using a WITec confocal Raman microscope (Alpha 300RS, Germany) equipped with a 532 nm laser diode (<30 mW), under an objective lens (100 × or others) at room temperature (~24 °C). In this test, we usually use the maximum laser power to collect the meaningful signal, which should be cautious to avoid the potential damage to the sample by the laser burning.

To map the image, the laser was scanning on the sample surface to collect the signal at each pixel or point. A previous study has demonstrated the capability of Raman imaging to analyse polystyrene nanoplastics down to 100 nm [20]. The methodology is validated and advanced herein to investigate the debris particles, particularly the ones smaller than 1 µm, or the nanoplastics, aided with the following algorithms.

2.2.1. PCA-based algorithm

The raw data from Raman scanning spectrum matrices were analysed by PCA in Origin (Pro 2022) software, as reported before [13], to regenerate the PCA spectrum via score (as y-axis, while the wavenumber as x-axis), and PCA image via loading coefficient (as z-axis, while the scanning pixel position as x/y-axis). Depending on the presentation orientation of the raw data array, the score and the loading coefficients can be swapped or transposed.

2.2.2. Algebra-based algorithm

Two or more images, no matter the mapped Raman intensity or PC loading coefficients, can be merged using algebra functions as well, including "SUBTRACT", "TIME", etc., using Origin software too [13]. In brief, we normalise the loading coefficient to 0–1 (such as using function "$(x_i - x_{min})/(x_{max} - x_{min})$"). We then subtract or time/multiply them with each other (as a merged one as z-axis) to generate a "merged" image.

2.3. Particle analysis

For particle analysis, ImageJ software was employed. Using ImageJ enabled the recognition of individual particles in complex aggregates or clusters, leading to an effective particle quantification [3]. After an image was opened in the software, the image background was subtracted using a suitable value (to clearly present and distinguish the to-be-targeted particles), and the random noise was removed by filter such as Gaussian blur. A colour threshold was adjusted to make almost every to-be-targeted particle identifiable; the image was made binary, followed by filling hole and watershed, and lastly the implementation of the particle analysis function [6]. The outlines of each particle can be extracted, and the particle area can be converted to size by root-squaring for statistical analysis, aided by Origin software again.
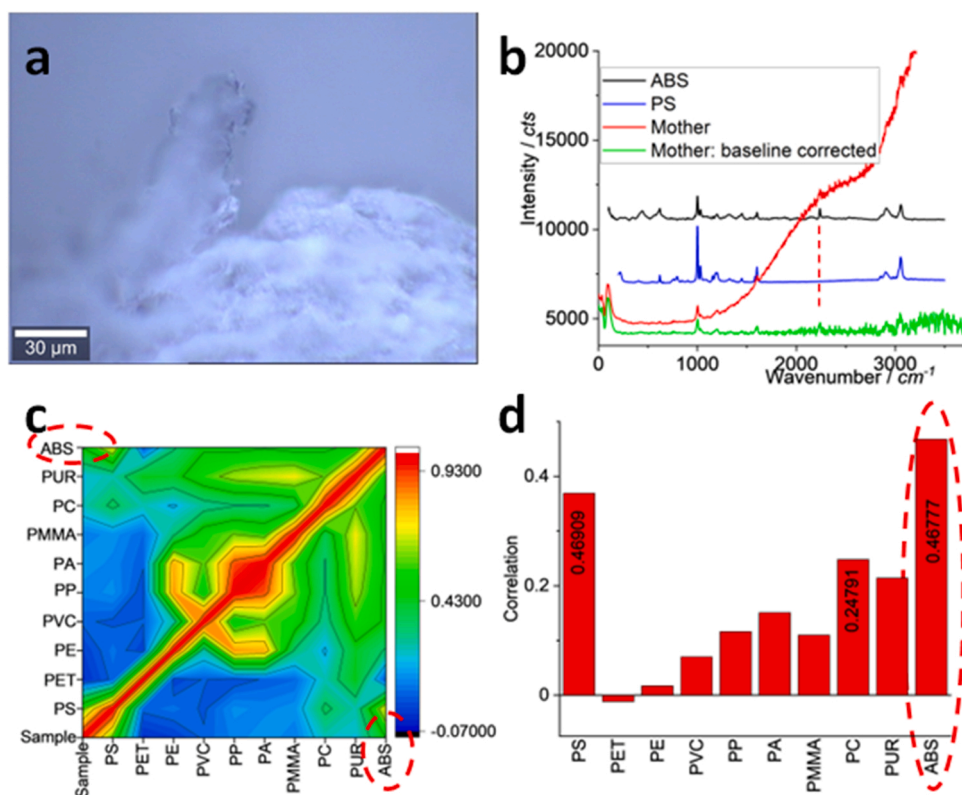
Fig. 2. Photo image (a), Raman spectra (b), correlation matrix (c), and correlation values (d). The assignment is indicated by circulating in (c, d).
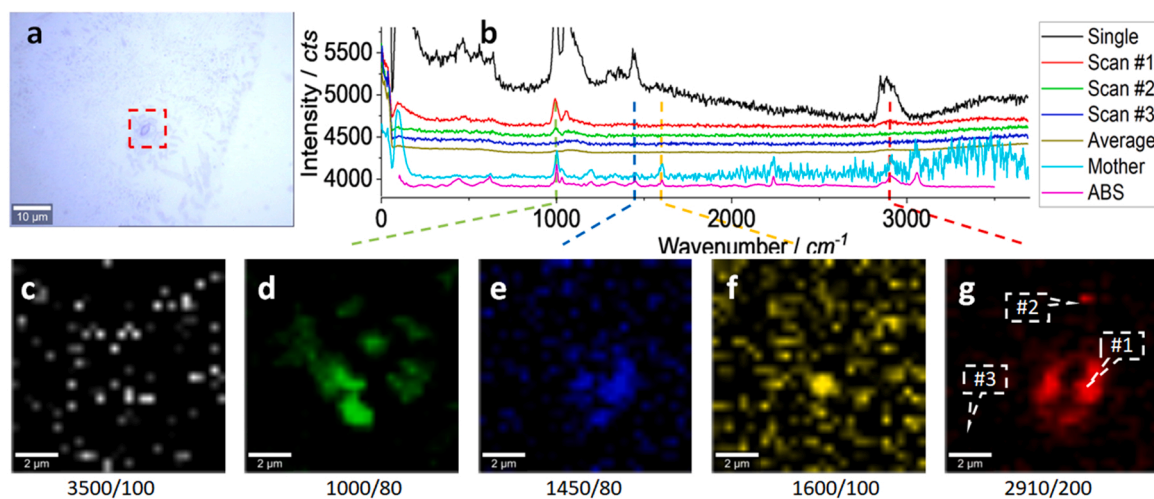

Fig. 3. Photo image (a), typical Raman spectra (b) and Raman intensity images (c-g). The squared area in (a) of 10 μm × 10 μm was scanned. Raman spectra were collected under an objective lens of 100 × , integration time of 1 s for each pixel of 0.33 μm × 0.33 μm (to create a matrix of 30 × 30). (b) shows the Raman spectra of ABS and the "mother" container, to compare with 1 single spectrum (10 s integration) and 3 typical scanning spectra (1 s) collected from the positions marked in (g), and their average spectrum of 900 (30 × 30) spectra. The intensity images (c-g) are mapped at a blank wavenumber window (c), the characteristic peaks of ABS (d-g), as marked under each image (and the peak width), after 10% colour off-setting.

2.4. Particle characterisation

An SEM (Zeiss Sigma VP) was used to characterise the morphology of the microplastics and nanoplastics, in addition to Energy-dispersive X-ray spectroscopy (EDS) detection. The sample was sputter-coated with a thin layer of platinum (~6 nm) to increase the conductivity. The accelerate voltage was 10–20 kV with a working distance 5–10 mm [5].

## 2. Results and discussion

3.1. SEM observation of debris in processed water samples

Fig. 1 shows the typical SEM images that we collected on the glass surface, leaving behind by a droplet of ~5 μL of the blender "juice" sample, once dried. In (a), we note there is a coffee ring and most of debris were concentrated along this ring [23,25]. The coffee ring is marked in (a) and we focus our test on it.
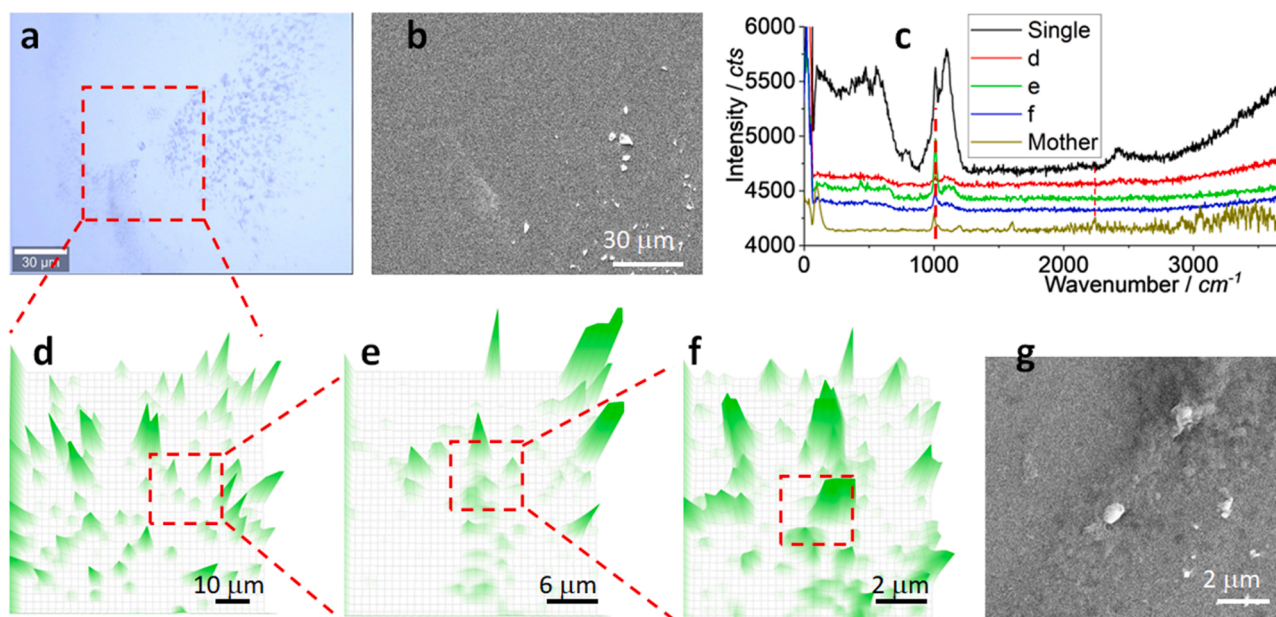
Fig. 4. Photo image (a), SEM images (b, g), Raman spectrum (c) and images (d-f) at different magnifications. The area in (a) of 80 μm × 80 μm was scanned and gradually zoomed in as (d-f), via the squared areas. Raman spectra were collected under an objective lens of 100 × , integration time of 1 s for each pixel of 2.7 μm × 2.7 μm (d), or 1 μm × 1 μm (e), or 0.33 μm × 0.33 μm (f) (to create a matrix of 30 × 30 in all cases). (b, g) shows the SEM images for comparison. (c) shows the Raman spectrum of "mother" container, to compare with a single spectrum (10 s) and 3 typical scanning spectra (1 s). The intensity images (d-f) are mapped at ~1000 cm^{-1} of ABS, using 3D presentation and white background. The squared area in (f) is further tested in Fig. 6.
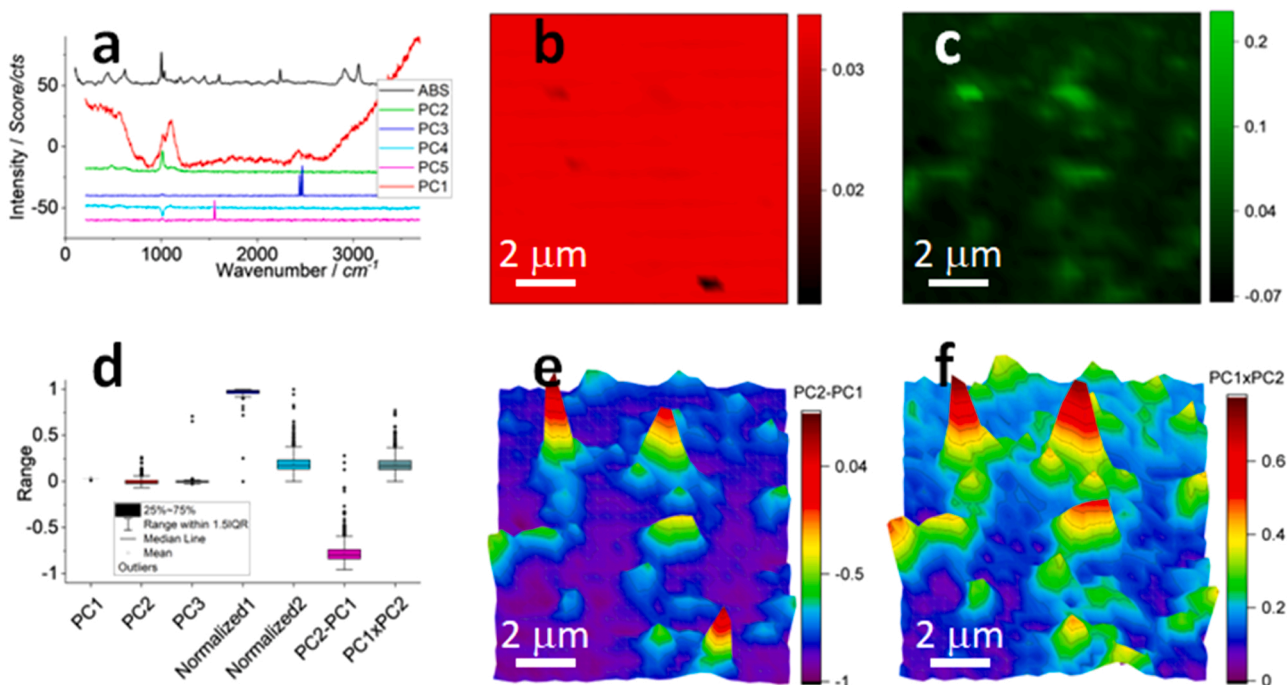

Fig. 5. PCA analysis on the raw spectrum matrix data in Fig. 4(f). (a) is the PCA spectrum, with ABS as a reference. (b, c) are the PCA images of PC1 and PC2, respectively. (d) shows the box plot of the loading coefficients, after normalised and merged, as indicated. (e, f) merge the images (b, c), using the indicated algebrafunctions on the colour scale bars.

Once zoomed in, Fig. 1(b) shows more details of the debris, from micro size to nano size, as presented in (c, d). Because there is no such kind of coffee ring from our control tests, the debris we collected in Fig. 1 is released from the blending process, particularly in the presence of ice blocks. Most likely, the blender generates a high-speed vortex in the container, which sends the ice blocks to scratch the container inner well and release debris. The detailed mechanism is beyond the scope of this research. In the following, we will test whether or not these debris are made of plastic, to confirm that the debris are either microplastics or nanoplastics.

3.2. Plastic identification: material of "mother" container

In this section, using Raman spectrum we identified container plastic
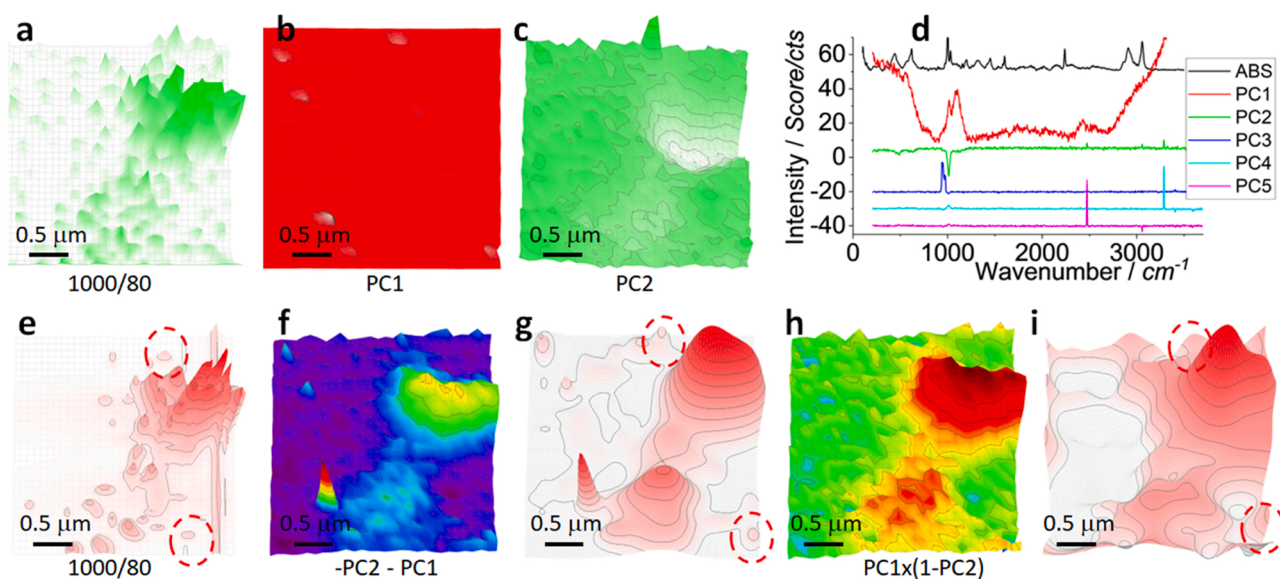
Fig. 6. Raman images (a, e), PCA images (b-c, f-i) and spectrum (d). (e, g, i) are other versions of (a, f, h), after image re-construction to enhance the signal-noise ratio. The squared area in Fig. 4(f) of 3 μm × 3 μm was scanned and Raman spectra were collected under an objective lens of 100 × , integration time of 1 s for each pixel of 0.1 μm × 0.1 μm (to create a matrix of 30 × 30). (b, c) show the PCA images of PC1 and PC2, respectively. (d) shows PCA spectrum, with reference of ABS. The intensity images (f, h) merge PC1 and PC2, as suggested under the images.

first, then using Raman imaging to capture microplastics and nanoplastics in Figs. 3–6.

To identify the container materials of polymers (obviously not glass nor stainless steel), we sampled the container outer wall first. The sample is shown in Fig. 2(a). The typical spectrum is shown in (b), with the spectrum of ABS as reference. From the sample's spectrum ("mother"), we can see that the strong background of fluorescence dominates the collected signal. Once the spectrum is pre-treated, such as to correct the baseline or the fluorescence background, the spectrum looks close to that of ABS [18].

This assignment can be further confirmed by a digital approach [13]. That is, we mixed this spectrum (after pre-treatment) with 10 common plastics' spectra, in order to correlate them via chemometrics. The correlate matrix is presented in Fig. 2(c). A "sword" pattern is symmetric along the diagonal, where each plastic is correlated with itself and generates a correlation value of 1. For our sample, only the right column or the bottom row is meaningful, which is extracted and presented in (d). We can see the highest correlation value of 0.46777 is generated for ABS, which leads us to assign the "mother" material of the container to ABS.

This assignment was conducted by selecting the maximum correlation value of 0.46777 to ABS (the second one is 0.36909 to PS). This domestic product might be not a pure ABS but a mixture with co-ingredients such as pigment or colorant, as evidence by the strong fluorescence in Fig. 2(b), which leads to the low correction value. Another possible reason, as suggested by the database (Rochman Lab), this ABS reference spectrum might be not a pure one because it has been also collected from domestic products, not from the pure sample. In the meantime, ABS has a similar spectrum with PS, but the peak at ~ 2240 cm^{-1} (marked by dashed line in b) can clearly distinguish them, which leads to the assignment to ABS, rather than PS.

In the following, we tested whether the debris particles in Fig. 1 released from the "mother" container (ABS) were microplastics/nanoplastics or not.

3.3. Raman imaging: microplastics and nanoplastics

3.3.1. Identification and visualisation of microplastics and nanoplastics
As mentioned, once a droplet is dried on the glass surface, a coffee ring is generally observed [23]. The testing on the central part is provided in Fig. S2 (Supporting Information). In this section and blow, we test the coffee ring area, as shown in Fig. 1.

Along the coffee ring, a photo image is shown in Fig. 3(a). In (b), the spectrum we collected (Single) is compared with the ABS spectrum and the "mother" container. The strong peaks appear at ~ 1000 cm^{-1} (in-plane deformation of the benzene ring), ~ 1450 cm^{-1}, ~ 1600 cm^{-1} (stretching vibration of the benzene ring) and ~ 2910 cm^{-1} (C-H), which leads to the assignment to ABS [18]. The peaks at ~ 1000 cm^{-1} and ~ 2910 cm^{-1} are stronger than the rests but the latter is usually shielded by the fluorescence background, so that the former should be paid more attention.

The single spectrum just suggests, at the signal collection position, the suspect is likely made of ABS. Other area remains unclear. We thus scan the squared area in Fig. 3(a), the typical spectra we collected are shown in (b), including a relative strong one (#1), a middle one (#2) and a weak one (#3) that was collected from the blank area as the spectrum background. Basically, the spectra of Scans #1–2 are similar with the single spectrum but with a lower signal intensity, due the short integration time (1 s vs. 10 s). The average spectrum from the whole spectrum matrix of 900 (30 × 30) spectra is also show. It looks similar with Scan #3, suggesting the scanning area is dominated by the blank (glass also emit scattering), echoing the image in (a).

From the scanning spectrum matrix that contains 900 spectra, we can map the characteristic peaks of ABS to directly visualise it. The signal-noise ratio can be significantly increased, from a statistical point of view. Before we map the characteristic peaks of ABS, we map a blank window where ABS has no contribution and generate an image in Fig. 3 (c). Only random noise is mapped, suggesting that Raman imaging can specifically capture targeted plastic via the characteristic peaks.

The characteristic peaks of ABS are mapped as images in Fig. 3(d-g). All have similar pattern, while (f) is blurred, due to the weak peak, as evidenced in (b). The rest images are clear, particularly in (d), suggesting the presence of ABS. The difference among them is due to different intrinsic intensity of the mapped characteristic peaks, and the spectrum background, as discussed above. In the meantime, the surface group of the particles might be derivate during the releasing process. We thus selected the peak at ~ 1000 cm^{-1} in the following to simplify the analysis. The specific positions to collect the spectra of scans #1–3 in (b)

are marked in (g). On the other hand, not every dot/particle in (a) has been mapped by Raman, due to the different imaging approach (e.g. photo and Raman). The reason will be detailed below.

3.3.2. Raman imaging: effect of scanning pixel size

In Fig. 4, we zoom in the scanning area to study the effect of the scanning pixel size. The SEM image in (b) looks a little different from photo image in (a), due to the slightly mis-matched position under the photo camera and the SEM. The typical spectra we collected are shown in (c), including a single spectrum with a longer integration time (10 s vs. 1 s). Two characteristic peaks are marked, from which we can basically assign them to ABS again.

Similarly, we map the images to visualise ABS microplastics and nanoplastics, with an increased signal-noise ratio. As discussed above, we focus the strong peak at ~1000 cm^{-1} and generate the images in Fig. 4(d-f), at different scanning area size or different magnifications. Basically, from (d) to (e) to (f), more detailed structures are mapped. We thus should balance between the low and the high magnifications, to see the overview and the details, the situation of which is similar with other microscopy too.

In Fig. 4(d), when the scanning is conducted with a pixel size of 2.7 μm × 2.7 μm, some fine structure might emit weak signal so that cannot be effectively picked up for imaging. On the contrary, in (e, f), the scanning pixel size has been decreased to 1 μm × 1 μm (e), or 0.33 μm × 0.33 μm (f). Consequently, the fine particles or structures can be mapped.

However, compared the Raman images in Fig. 4(d-f) with the SEM images in (b, g), the difference is still there, although they are basically matched. Particularly when compared (f) with (g), not every particle in the SEM image is mapped by Raman. That is because the different imaging approach, SEM has a much higher resolution (nm or sub) than Raman, using electron beam to collect the secondary electron, while Raman uses laser to emit the spectrum. From Raman imaging, herewith we used an objective lens of 100 ×, the imaging resolution (or the recommended scanning pixel size) is controlled by the laser diffraction, at *λ/2NA*, ~300 nm because the wavelength of *λ* is 532 nm and the numerical aperture *NA* is 0.9. That is, to image the nanoplastics that generally have a weak signal, we should decrease the scanning pixel size to zoom in the scanning area, to enable the central part of the laser spot (with the size of ~300 nm where the energy density is much higher than the off-central area, following a Gaussian surface) to excite the Raman scattering, towards the effective imaging. Even so, the imaging resolution of Raman is not comparable with that of SEM, which leads to the difference.

3.3.3. PCA analysis of Raman raw data

The above solo peak's imaging might suffer the bias, meaning a low imaging certainty. A chemometrics of PCA has been recently employed to directly decode the scanning Raman spectrum matrix, for the whole set of spectrum rather than a solo peak, to participate the imaging process. That is, ideally, PCA can orthogonally decompose the matrix to two new matrices, one containing the spectrum profile information (score) while another containing the intensity information (PCA intensity for the loading coefficient). The former can generate the PCA spectrum, while the latter can be mapped as image (PCA image), to take all contributions from the whole set of spectrum. Using this approach we analysis the raw data in Fig. 4(f) and the results are presented in Fig. 5.

In Fig. 5(a), the PCA spectrum of PC1 is dominated by the spectrum background that looks similar with the scan #3 in Fig. 3(b), to generate a non-flat baseline with two broad peaks at ~1100 cm^{-1} and ~2430 cm^{-1} that are assigned to glass background. The peak at ~1000 cm^{-1} is also observed, suggesting that PC1 also contains the contribution from the ABS plastic. PC2 has a flat baseline and dominated by the peak at ~1000 cm^{-1}, suggesting the main contribution from ABS. The rests look like the noise, or the PCA calculation deviations. More PCA parameters are provided in Fig. S3 (Supporting Information).

We map the loading coefficients of PC1 and PC2 to generate images in Fig. 5(b, c). Again, PC1′ image in (b) is dominated by the image background, while PC2′s image in (c) is dominated by the plastic ABS. (c) looks like Fig. 4(f), further confirming the presence of ABS and suggesting the success of PCA analysis.

Since both PC1 and PC2 contain the contribution from ABS, due to the appearance peak at ~1000 cm^{-1}, we thus can merge them to pick up the un-supervised PCA analysis signal, to intentionally correct the non-supervised results [4,13]. To this end, we need pre-teat the PCA intensity or the loading coefficients first, as suggested in Fig. 5(d). By normalising them to the same range of 0–1, the different eigenvalue percentages can be intentionally corrected, to avoid the bias.

Using the normalised loading coefficients, we can merge them to generate images in Fig. 5(e, f), to pick up both contributions from PC1 and PC2. In (e), we take PC1 image as background to correct the PC2 image, using an algebra function of "PC2 – PC1″". In (e), we time or multiply them together, using "PC1 × PC2″", to enlarge and emphasis the similar part (at the same pixel) from PC1 and PC2, seemingly originating from the peak at ~1000 cm^{-1} that appeared in PC1 and PC2. In both cases, the images in (e, f) are similar with that in Fig. 4(f), suggesting the success on the further treatment. Note, herewith the image certainty has been further increased, when compared with the images in Fig. 5(c), 4 (f).

3.3.4. High resolution and image re-construction towards deconvolution

We further zoom-in the scanning area squared in Fig. 4(f) and the results are presented in Fig. 6. The size of the scanning pixel (100 nm × 100 nm) is much smaller than the recommended one at ~300 nm. In this case, by shrinking the scanning size, we hopefully capture more detailed structures, because the centroid of the laser (a Gaussian surface) will have more chance to excite the stronger signal. In Fig. 6(a), a Raman image is presented as a reference, by mapping the strongest peak at ~1000 cm^{-1}, as discussed above.

Once PCA is conducted, the PC1-PC2 images are shown in Fig. 6(b, c). Compared with (a), a reversed pattern is observed from (c), while (b) looks like the background. That, the pattern in (a) is mapped as a "hole" in (c). The reason is due to the reversed peak at ~1000 cm^{-1} in (d) for PC2, suggesting the important of further treatment on the non-supervised PCA. Other PCs' images and analysis parameters are provided in Fig. S4 (Supporting Information).

Similarly, we employ algebra function to further treat the PCA results and present them as images in Fig. 6(f, h). Due to the PC2′s reversed peak at ~1000 cm^{-1} in (c, d), we correct the loading coefficient of PC2 either with (−1) in (f), or (1-PC2) in (h), after being normalised them to 0–1. The patterns in (f, h) are thus similar with that in (a), to visualise the ABS nanoplastics, particularly in (h).

In Fig. 6(a, f, h), the noise might be strong, which can lead to the false image. The reason is either due to the decreased scanning pixel to 100 nm × 100 nm, smaller than the recommended one (~300 nm), or owing the small size or cross-section of nanoplastic. To remove this noise, we can either off-set the colour or re-construct the image via deconvolution. In the latter case, a similar approach with FINOA was reported to realise a super-resolution imaging [24]. Using the similar approach, we re-construct the images (a, f, h) to images (e, g, i), by fitting as Gaussian surface in 2D. Basically they match well with these images before the re-construction. However, the noise can be significantly decreased by the fitting, which can either filter the noise (not pick up towards fitting) or average the random noise (pick up as background). In (e), the vertical line on the right boundary originating from the boundary effect should be ignored. In (g, i), two big particles (top-right one and middle-bottom one) are re-constructed with a smooth surface, which is different from (e), originating from the extra contribution of the PCA-algebra algorithm. Several particles are simultaneously images in (e, g, i), the circulated ones. In this case, we can assign them to nanoplastics that were released from the blender. More fitting details are provided in Fig. S5, Tables S1-S3 (Supporting Information).
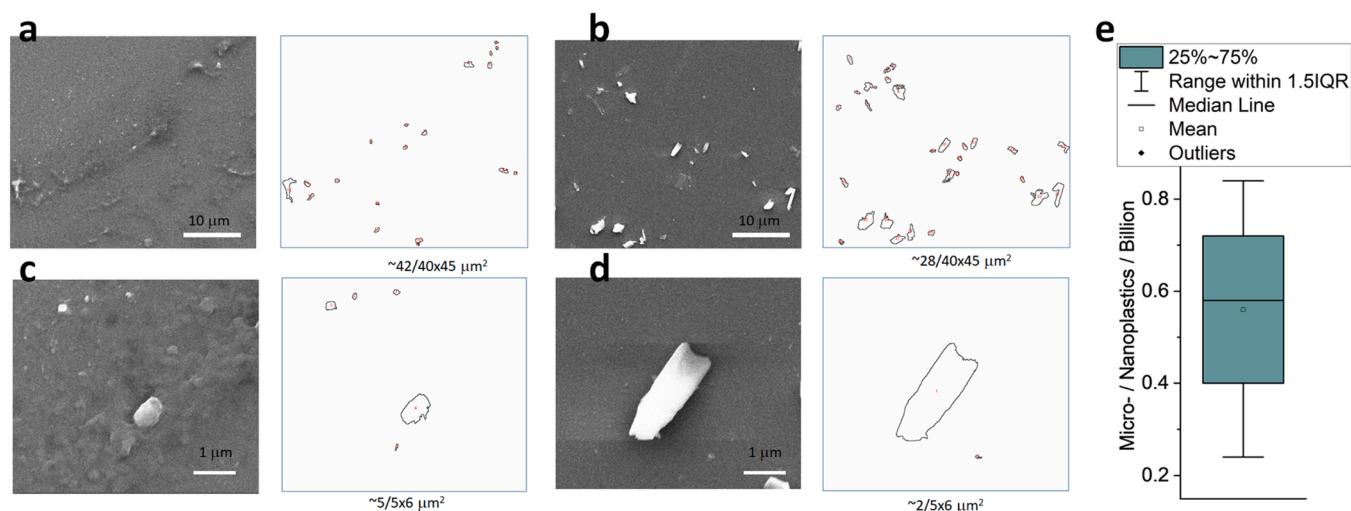
Fig. 7. Microplastic and nanoplastic counting with help of ImageJ. Four typical SEM images (a-d) are analysed, the particle outlines are presented on the right for comparison. The number of the particle and the size of the SEM images are indicated. (e) is the statistical analysis for a run (30 s) of blender.

3.4. Particle analysis for estimating the amount of plastic debris released

Herein we analysed the amount of the particles released, using software ImageJ. Four typical SEM images recorded from the "coffee ring" area were analysed in Fig. 7. The outlines of the targeted particles are shown for comparison, along with the image size. Basically, ~0.16 particle/μm^2 is released by averaging them.

In Fig. 1, the droplet of ~5 μL dried on glass slide surface, left behind a pattern of a "coffee ring" with a diameter 5–10 mm (D). The thickness / width of the coffee ring is estimated at 50 ~μm (d). Therefore, the coffee ring has an area of πDd, 0.78–1.6 $\times 10^6$ μm^2, to cover ~0.12–0.26 $\times 10^6$ particles (using the density of ~0.16 particle/μm^2). This droplet of ~5 μL was sampled from ~15 mL concentrated liquid from a run of blending, and this means the blending process of 30 s might release ~0.36–0.78 $\times 10^9$ microplastics and nanoplastics. This amount is significant and might be underestimated, because the central part of the droplet beyond the "coffee ring" was not counted.

This estimate has variations depending on the materials and features of the blender (container, speed, working mechanism/configuration etc.), food materials (hardness/shape/size/amount), blending duration, temperature, presence of ice block (shape/size/amount) etc. The software ImageJ results may also experience discrepancy, such as from the background selection, colour threshold, size adjustment etc.[6]. Our results clearly suggests that the blender can be a source of microplastics and nanoplastics in our kitchen. Since the plastic debris are directly present in our food and might enter our digestion system, we should be very cautious to use the blender in our kitchen, given the risk assessment has not yet been conducted. Another material, such as glass and stainless steel, is thus recommended.

4. Conclusion

The characterisation of microplastics and nanoplastics is still faced with some challenges. We suggest that the Raman imaging can be a suitable approach for future research, by balancing between the advantages and the disadvantages. Specifically, the Raman imaging works like a microscopy, if the signal is well extracted and interpreted: zooming in can capture details such as nanoplastics, and zooming out can provide overview of a big area. Once zoomed-in, however, the signal should be well justified to avoid the potential bias, such as via image algorithm. The combination of morphology analysis with chemical identification, such as combining SEM-Raman in the same platform, should be another approach to be explored, towards the instrument

integration. Further research is also needed to address this balance towards broader applications.

Currently we have advanced Raman imaging to capture microplastics and particularly nanoplastics released from a kitchen blender. The significant releasing amount sends us a strong warning that we should be careful to use blenders to make juice or to smash food. Microplastics and nanoplastics is a vast but hardly visible issue, and we are potentially exposed to them to a greater extent than we perceive. Risk assessment is therefore recommended in support of management and regulation targeted at plastic product safety.

CRediT authorship contribution statement

The authors: Cheng Fang, Ravi Naidu, were involved in experiment design and management. The authors: Cheng Fang, Yunlong Luo, participated in data collection and sample preparation. The authors: Yunlong Luo, Olalekan Simon Awoyemi helped the manuscript preparation and reviewing process.

Environmental Implication

This study presents characterisation of microplastics and nanoplastics released from a little-known source (i.e. kitchen blenders). The results expand the existing scientific knowledge of plastic contamination resulting from everyday activities. The blender-derived plastic debris might contaminate the food processed in the blenders, underscoring an urgent need for comprehensive risk assessment. The microplastics and nanoplastics are also likely to go down the kitchen sink after blenders are washed, and then end up in the sewage system.

Declaration of Competing Interest

The authors declare that they have no known competing financial interests or personal relationships that could have appeared to influence the work reported in this paper.

Data Availability

No data was used for the research described in the article.

Acknowledgements

University of Newcastle, Australia. For the Raman measurements and SEM, we also acknowledge the use and support of the South Australian node of Microscopy Australia (formerly known as AMMRF) at Flinders University, South Australia.

Appendix A. Supporting information

References

[1] Ageel, H.K., Harrad, S., Abdallah, M.A.-E., 2022. Occurrence, human exposure, and risk of microplastics in the indoor environment. Environ Sci Process Impacts 24 (1), 17–31.

[2] Araujo, C.F., Nolasco, M.M., Ribeiro, A.M.P., Ribeiro-Claro, P.J.A., 2018. Identification of microplastics using Raman spectroscopy: latest developments and future prospects. Water Res 142, 426–440.

[3] Bescond, A., Yon, J., Ouf, F.X., Ferry, D., Delhaye, D., Gaffié, D., Coppalle, A., Rozé, C., 2014. Automated determination of aggregate primary particle size distribution by TEM image analysis: application to soot. Aerosol Sci Technol 48 (8), 831–841.

[4] Cheng, F., Luo, Y., Naidu, R., 2022. Raman imaging combined with an improved PCA/algebra-based algorithm to capture microplastics and nanoplastics. Analyst 147 (19), 4301–4311.

[5] Cowger, W., Booth, A.M., Hamilton, B.M., Thaysen, C., Primpke, S., Munno, K., Lusher, A.L., Dehaut, A., Vaz, V.P., Liboiron, M., Devriese, L.I., Hermabessiere, L., Rochman, C., Athey, S.N., Lynch, J.M., De Frond, H., Gray, A., Jones, O.A.H., Brander, S., Steele, C., Moore, S., Sanchez, A., Nel, H., 2020. Reporting guidelines to increase the reproducibility and comparability of research on microplastics. Appl Spectrosc 74 (9), 1066–1077.

[6] Crawford, E.C., Mortensen, J.K., 2009. An ImageJ plugin for the rapid morphological characterization of separated particles and an initial application to placer gold analysis. Comput Geosci 35 (2), 347–359.

[7] Gall, S.C., Thompson, R.C., 2015. The impact of debris on marine life. Mar Pollut Bull 92 (1), 170–179.

[8] Ivleva, N.P., 2021. Chemical analysis of microplastics and nanoplastics: challenges, advanced methods, and perspectives. Chem Rev 121 (19), 11886–11936.

[9] Käppler, A., Fischer, D., Oberbeckmann, S., Schernewski, G., Labrenz, M., Eichhorn, K.-J., Voit, B., 2016. Analysis of environmental microplastics by vibrational microspectroscopy: FTIR, Raman or both? Anal Bioanal Chem 408 (29), 8377–8391.

[10] Leal Filho, W., Saari, U., Fedoruk, M., Iital, A., Moora, H., Klöga, M., Voronova, V., 2019. An overview of the problems posed by plastic products and the role of extended producer responsibility in Europe. J Clean Prod 214, 550–558.

[11] Leslie, H.A., J. M. van Velzen, M., Brandsma, S.H., Vethaak, D., Garcia-Vallejo, J.J., Lamoree, M.H., 2022. Discovery and quantification of plastic particle pollution in human blood. Environ Int, 107199.

[12] Luo, H., Liu, C., He, D., Xu, J., Sun, J., Li, J., Pan, X., 2022. Environmental behaviors of microplastics in aquatic systems: a systematic review on degradation, adsorption, toxicity and biofilm under aging conditions. J Hazard Mater 423, 126915.

[13] Luo, Y., Zhang, X., Zhang, Z., Naidu, R., Fang, C., 2022. Dual-principal component analysis of the Raman spectrum matrix to automatically identify and visualize microplastics and nanoplastics. Anal Chem 94 (7), 3150–3157.

[14] Lusher, A., Hollman, P., Mendoza-Hill, J., 2017. Microplastics in Fisheries and Aquaculture: Status of Knowledge on Their Occurrence and Implications for Aquatic Organisms and Food Safety. FAO.

[15] Marazuela, M.D., Klaiber, M., Moreno-Gordaliza, E., Barata, A., Gómez-Gómez, M. M., 2022. Safety assessment of commercial antimicrobial food packaging: Triclosan and microplastics, a closer look. Food Packag Shelf Life 31, 100780.

[16] Margasahayam, A., Balraj, Y., 2018. Properties of food ingredients during processing in a domestic mixer grinder and subsequent storage: a review. J Food Process Eng 41 (4), e12677.

[17] Pattammattel, A., Kumar, C.V., 2015. Kitchen chemistry 101: multigram production of high quality biographene in a blender with edible proteins. Adv Funct Mater 25 (45), 7088–7098.

[18] Reggio, D., Saviello, D., Lazzari, M., Iacopino, D., 2020. Characterization of contemporary and historical acrylonitrile butadiene styrene (ABS)-based objects: Pilot study for handheld Raman analysis in collections. Spectrochim Acta Part A: Mol Biomol Spectrosc 242, 118733.

[19] Sobhani, Z., Lei, Y., Tang, Y., Wu, L., Zhang, X., Naidu, R., Megharaj, M., Fang, C., 2020. Microplastics generated when opening plastic packaging. Sci Rep 10 (1), 4841.

[20] Sobhani, Z., Zhang, X., Gibson, C., Naidu, R., Mallavarapu, M., Fang, C., 2020. Identification and visualisation of microplastics/nanoplastics by Raman imaging (i): down to 100 nm. Water Res, 115658.

[21] Soltani, N.S., Taylor, M.P., Wilson, S.P., 2021. Quantification and exposure assessment of microplastics in Australian indoor house dust. Environ Pollut 283, 117064.

[22] Soltani, N.S., Taylor, M.P., Wilson, S.P., 2022. International quantification of microplastics in indoor dust: prevalence, exposure and risk assessment. Environ Pollut 312, 119957.

[23] Wong, T.-S., Chen, T.-H., Shen, X., Ho, C.-M., 2011. Nanochromatography driven by the coffee ring effect. Anal Chem 83 (6), 1871–1873.

[24] Yildiz, A., Forkey, J.N., McKinney, S.A., Ha, T., Goldman, Y.E., Selvin, P.R., 2003. Myosin V walks hand-over-hand: single fluorophore imaging with 1.5-nm localization. Science 300 (5628), 2061–2065.

[25] Yunker, P.J., Still, T., Lohr, M.A., Yodh, A.G., 2011. Suppression of the coffee-ring effect by shape-dependent capillary interactions. Nature 476, 308.

[26] Zhang, Q., Zhao, Y., Du, F., Cai, H., Wang, G., Shi, H., 2020. Microplastic fallout in different indoor environments. Environ Sci Technol 54 (11), 6530–6539.

[27] Zhao, S., Danley, M., Ward, J.E., Li, D., Mincer, T.J., 2017. An approach for extraction, characterization and quantitation of microplastic in natural marine snow using Raman microscopy. Anal Methods 9 (9), 1470–1478.